Deng, Q.; Smetanin, M.; Weissmueller, J.:
Mechanical modulation of reaction rates in electrocatalysis
In: Journal of Catalysis (2013) Elsevier

DOI: 10.1016/j.jcat.2013.10.008

Mechanical modulation of the electrocatalytic hydrogen evolution reaction

Qibo Deng[1], Maxim Smetanin[2], Jörg Weissmüller[1,3,*]
1–Institut für Werkstoffphysik und Werkstofftechnologie, Technische Universität Hamburg-Harburg, Hamburg, Germany
2–Department of Chemistry , University of Guelph, Guelph, Canada
3–Institut für Werkstoffforschung, Werkstoffmechanik, Helmholtz-Zentrum Geesthacht, Geesthacht, Germany and
** email weissmueller@tuhh.de*

The paper explores how changes in the lattice parameter at an electrode surface by elastic strain affect the catalytic activity. The focus is on the hydrogen evolution reaction on 111-textured, polycrystalline Au and Pt thin film electrodes in H_2SO_4 as a model process. A lock-in technique allows the modulation of the reaction current to be measured in situ during small cyclic strain imposed on the electrode. While tensile strain enhances the exchange current density and the reactivity at low overpotential, ΔE, the trend is inverted and the reactivity diminished at higher ΔE. Strain is introduced into the kinetic rate equation for Heyrowsky kinetics by allowing for strain-dependence of the hydrogen adsorption enthalpy as well as the activation enthalpy. The results link the current modulation to electrocapillary coupling coefficients that are open to investigation by experiment or computer simulation. The inversion in sign of the coupling as the function of ΔE emerges in agreement with experiment.

I. INTRODUCTION

Advanced materials for heterogeneous catalysis are often alloys in which an active component is enriched in the surface layer of atoms. Core-shell nanoparticles provide an example for such compositionally graded systems. An inherent feature of those catalysts is that the atoms of the active component at the surface do not, in general, see the same interatomic spacing as in their elemental crystalline state. It is therefore significant that density function theory (DFT) calculations [1–4] suggest that reaction rates in heterogeneous catalysis vary considerably when the surface is elastically strained in the tangent plane. The suggested strain-dependence rests on computed values for the adsorption enthalpies of the reactants on strained surfaces, which are found to be significantly modified. That finding has been experimentally confirmed [5–7]. Enhanced reaction rates on strained catalyst layers have also been reported in experimental studies [8–10]. The electronic structure in the active layer at compositionally graded surfaces is affected by electron exchange with the underlying substrate, and this 'ligand effect' affects the reactivity simultaneously with the lattice parameter change. Since the two effects are not readily separated, the impact of strain is not typically observed in isolation. In fact, quantifiable measures for the reactivity-strain coupling strength have not been reported so far, nor are definitions for the coupling parameters established.

Here, studying the hydrogen evolution reaction (HER) as a model process, we introduce the strain-dependence into a rate equation for electrocatalysis and we present an experimental approach towards isolating and quantifying the coupling between strain and reaction rate. The results advertise that the mechanical modulation of the catalytic reactivity is governed by strain-dependent values of the adsorption enthalpy and activation enthalpy and they point the way towards measuring the relevant enthalpy-strain coupling coefficients in experiment.

The impact of strain on electrode processes has been explored for ideally polarizable electrodes, where it is measured by the electrocapillary coupling parameter, ς. This quantity is defined as the response of the electrode potential, E, to strain at constant charge density. Important contributions to defining and measuring ς have been made in the 1970s by AY Gokhshtein [11], but the subject has found little attention until much later Haiss [12] related ς of nominally clean surfaces near their potential of zero charge (pzc) to the electronic structure of the metal surface and to charge transfer with adsorbates. More recent experiments have confirmed that notion [13, 14], and have received support by ab-initio computation [15, 16]. The value of ς varies with E and is characteristic for individual electrode processes. It has been shown that the ς-value of an electrosorption process measures the strain-dependence of the corresponding adsorption enthalpy [7]. Since adsorption strength is a key issue in heterogeneous catalysis, the electrocapillary coupling parameters are of immediate relevance for understanding the impact of strain on the catalytic activity of a surface.

We have previously reported how ς for polarizable electrodes can be measured by dynamic electro-chemomechanic analysis (DECMA). That method rests on fast cyclic straining of electrodes during the much slower potential scans of cyclic voltammetry [17]. The strain creates a modulation of the electrode potential, which can be isolated by a lock-in amplifier and evaluated in terms of $\varsigma(E)$. In the experimental part of this paper, we explore a generalization of DECMA where the modulation of the Faraday current is monitored while the electrode is cyclically strained during an electrocatalytic reaction. The experiment is complemented by the introduction of a rate equation, which affords predictions on how the strain-dependent adsorption and activation enthalpies af-

fect the reactivity, and which is open to comparative discussion in relation to experiment.

II. THEORY

We start out by briefly establishing the terminology for discussing our experiments; for more details see Refs. [17, 18]. We consider elastic deformation quantified by the strain variable $e = \delta\tilde{A}/\tilde{A}$ with $\tilde{A}$ the physical area of the electrode surface. A cyclic elastic strain is imposed according to

$$e = \hat{e}\sin(\omega t) \tag{1}$$

while the electrode potential, E, is held constant. The symbols t, ω, and $\hat{e}$ denote time, frequency, and strain amplitude. The task is to analyze the modulation of the reaction current in response to the cyclic strain. This requires a distinction between capacitive or pseudocapacitive processes on the one hand and Faraday reactions on the other.

We first consider an ideally polarizable electrode at equilibrium, and assume a surface excess free energy function $\psi(q, e)$ with the state variables q, the interfacial charge density, and e, and with the fundamental equation $\mathrm{d}\psi = E\mathrm{d}q + f\mathrm{d}e$. We use Lagrange coordinates, measuring all densities (and specifically ψ, q, and the current density, j) per area of the undeformed electrode surface [18]. Two relevant materials parameters (i.e., second derivatives of ψ) are the differential capacitance, $c = \mathrm{d}q/\mathrm{d}E|_e$, and the electrocapillary coupling coefficient,

$$\varsigma = \mathrm{d}E/\mathrm{d}e|_q. \tag{2}$$

It is also readily shown [17] that the charge modulation at constant potential is

$$\mathrm{d}q/\mathrm{d}e|_E = -c\varsigma\,. \tag{3}$$

In terms of the above coefficients, cyclic strain experiments on polarizable electrodes near equilibrium, with either the charge or the current held constant result, respectively, in the potential- or current modulation

$$E = \varsigma\hat{e}\sin(\omega t) \qquad (\text{constant } q)\,, \tag{4}$$

$$j = -\varsigma c\,\omega\hat{e}\cos(\omega t) \qquad (\text{constant } E)\,. \tag{5}$$

DECMA experiments have verified that ς can be consistently measured by each of the two experimental approaches [17].

We now turn to non-equilibrium processes and start out by assuming that the specific charge density q remains well-defined there. The net current density (current per area) can then be decomposed into pseudocapacitive ($j^{\mathrm{pc}} = \mathrm{d}q/\mathrm{d}t$) and Faraday ($j^{\mathrm{F}}$) current contributions according to

$$j = \mathrm{d}q/\mathrm{d}t + j^{\mathrm{F}}(E, e)\,. \tag{6}$$

The expression $j^{\mathrm{F}} = j^{\mathrm{F}}(E, e)$ is our constitutive assumption for the Faraday current. With attention to small strain, as in a DECMA experiment, the expression can be expanded to first order as $j^{\mathrm{F}}(E, e) = j_0^{\mathrm{F}}(E) + \iota e$, with

$$\iota = \mathrm{d}j^{\mathrm{F}}/\mathrm{d}e|_E \tag{7}$$

a current-strain coupling coefficient. As will become apparent below, it is also of interest to introduce an alternative measure for the current-strain coupling in the form of the coefficient λ, defined as

$$\lambda = \frac{RT}{F}\frac{1}{j^{\mathrm{F}}}\frac{\mathrm{d}j^{\mathrm{F}}}{\mathrm{d}e}|_E\,. \tag{8}$$

This parameter measures the relative variation (variation of $\ln j^{\mathrm{F}}$) of the Faraday current.

The notation introduced so far lets us write

$$j = j_0^{\mathrm{F}} - \varsigma c\,\omega\hat{e}\cos(\omega t) + \iota\hat{e}\sin(\omega t). \tag{9}$$

for the modulated current during strain cycles at constant potential. The first term on the right-hand side of Eq (9) is the Faraday current at $e = 0$, the second term originates from pseudo-capacitive processes, and the third term is the modulated Faraday current.

With attention to experiments at small strain (in the present work, $e \leq 10^{-3}$) we take all materials parameters in Eq (9) as evaluated at $e = 0$ and focus on their potential-dependence alone. Thus, $c = c(E)$, $\varsigma = \varsigma(E)$, $\iota = \iota(E)$, and $\lambda = \lambda(E)$.

Equation (9) suggests characteristic signatures of the pseudocapacitive and Faraday processes which afford their separation in experiment: The pseudo-capacitive modulated current is phase-shifted by 90° relative to the strain, whereas the modulated Faraday current is in phase. Furthermore, the modulated pseudo-capacitive current scales with the frequency, whereas the modulated Faraday current is invariant during frequency change.

With attention to the hydrogen evolution reaction (HER) on Au and Pt we explore strain-dependence under the assumption that the rate-controlling step may be taken as the ion+atom (Heyrowsky) reaction, $\mathrm{H}^+_{\mathrm{aq}} + \mathrm{H}_{\mathrm{ad}} + \mathrm{e}^- \rightleftharpoons \mathrm{H}_{2,\mathrm{ad}}$ [19, 20], using the results by Parsons [21] for the reaction kinetics. The H_2 desorption step as well as the discharge (Volmer) reaction, $\mathrm{H}^+_{\mathrm{aq}} + \mathrm{e}^- \rightleftharpoons \mathrm{H}_{\mathrm{ad}}$, are taken to be fast. Consistent with that assumption, the coverage θ with hydrogen is assumed to take on the equilibrium value of the Langmuir isotherm,

$$\theta^{\mathrm{L}} = \left(1 + \exp\frac{\Delta g^{\mathrm{ad}} + F\Delta E}{RT}\right)^{-1}\,. \tag{10}$$

with

$$\Delta g^{\mathrm{ad}} = \Delta h^{\mathrm{ad}} - T\Delta s_0^{\mathrm{ad}} \tag{11}$$

the free energy of adsorption. The symbols have the following meaning: ΔE - overpotential, F - Faraday constant, R - gas constant, T - temperature. All molar quantities are per mole of H. The adsorption enthalpy Δh^{ad}

represents the change in molar enthalpy for the reaction $\frac{1}{2}H_2^{gas} \rightarrow H^{ad}$ (see Fig. 1), and Δs_0^{ad} refers to the corresponding entropy change, accounting for the entropies in the gas and for a θ-independent vibrational entropy of the adsorbed H, but excluding the configurational entropy of the adsorbate phase. Figure 2 is a schematic display of selected quantities of the model, showing the Langmuir isotherm in part a).

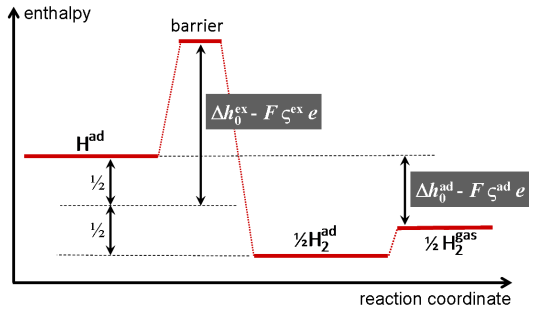

FIG. 1. Schematic representation of enthalpy terms in the rate-equation for the Heyrowsky reaction with symmetry factor 1/2. The small strain e is taken to affect the values of the adsorption enthalpy Δh^{ad} and of the barrier height Δh^{ex} through the coupling parameters ς^{ad} and ς^{ex}, respectively.

For conciseness, we assume that energies vary symmetrically with the reaction coordinate, so that the symmetry parameter is $\alpha = 1/2$. Parsons' [21] expression for the Faraday current can then be written in the form (see, for instance, Ref. [22])

$$j^F = j^{ex}\left\{\frac{1-\theta}{1-\theta_{eq}}\exp\left(\frac{F\Delta E}{2RT}\right) - \frac{\theta}{\theta_{eq}}\exp\left(\frac{-F\Delta E}{2RT}\right)\right\} \quad (12)$$

with θ_{eq} the coverage at the equilibrium potential of the HER and j^{ex} the exchange current density,

$$j^{ex} = \text{const.}\exp\left(-\frac{\Delta h^{ex}}{RT}\right). \quad (13)$$

The activation enthalpy Δh^{ex} relates to the energy barrier for the combination of proton and adsorbed hydrogen (see Fig. 1). Figure 2 b) shows a schematic Tafel plot for the HER. It is noteworthy that the "Tafel slope", $\mathrm{d}/\mathrm{d}\ln j^F$, changes at the potential, E^{ad}, of electrosorption.

The terms $F\Delta E$ in the kernels of the exponentials in Eq (12) represent the driving force for the reaction. The driving force is independent of the strain of the electrode, since the reactants and products are in solution. Our central assumption is that the impact of strain on the Heyrowsky reaction is mediated by two factors, namely *i*) a strain-dependence of the activation enthalpy for the ion+atom reaction step, and *ii*) a strain-dependence of the hydrogen adsorption enthalpy.

It is advantageous to define the response parameters, ς^{ad} and ς^{ex}, for the enthalpies so that they correspond to the potential-strain response in certain limiting

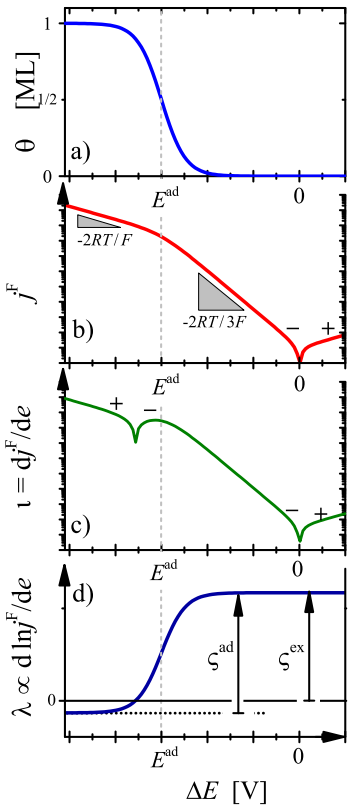

FIG. 2. Schematic representation of variation, as the function of overpotential, ΔE, of quantities relevant for the discussion of Heyrowsky reaction kinetics: **a.)**, surface hydrogen coverage, θ. **b.)**, Tafel plot of current density, j^F. Note change in Tafel slope (as indicated by labels) at the potential, E^{ad}, of hydrogen electrosorption. **c.)**, current-strain response, ι. **d.)**, current-strain coupling coefficient, λ. A jump in λ by the amount ς^{ad} concurs with the transition between dilute ($\theta \ll 1$) and concentrated ($\theta \approx 1$) hydrogen adsorbate population at E^{ad}. ς^{ad} and ς^{ex} measure the strain-dependence of the H adsorption enthalpy and the activation barrier energy, respectively. The graph of $\lambda(E)$ also depends on the strength of adsorption, see main text and Table I.

cases. This is achieved by expressing the strain response through [7]

$$\Delta h^{ad} = \Delta h_0^{ad} - F\varsigma^{ad}e\,, \quad (14)$$
$$\Delta h^{ex} = \Delta h_0^{ex} - F\varsigma^{ex}e\,. \quad (15)$$

The strain-dependence of Δh^{ad} affects the Faraday current of Eq (12) in as much as the coverages become strain-dependent, and here specifically $\theta = \theta^L(E, e)$. It is important to note that the strain-dependence needs to be carried through to the coverage at the equilibrium potential. Otherwise, the principle of detailed balance would be violated for the strained surface and the reaction current at equilibrium deviate from zero. Thus, we have also $\theta_{eq} = \theta^L(E_{eq}, e)$.

TABLE I. Values of the reaction rate-strain coupling coefficient λ as predicted by Eq (16) for the Heyrowsky reaction on surfaces with different free energy of adsorption, Δg^{ad}, for hydrogen. Examples for relevant materials are indicated in brackets. The three limiting cases of the overpotential, ΔE, refer to concentrated (coverage $\theta \approx 1$) and dilute ($\theta \ll 1$) hydrogen adsorbate and to the equilibrium of the hydrogen evolution reaction, $\Delta E = 0$, where the results shown apply irrespective of the value of θ. Electrocapillary coupling parameters for the activation barrier of the Heyrowsky reaction and for the hydrogen adsorption enthalpy are denoted by ς^{ex} and ς^{ad}, respectively. Note that λ jumps by $-\varsigma^{\mathrm{ad}}$ when the surface undergoes the transition from dilute to concentrated adsorbate during hydrogen electrosorption.

	$\Delta E \ll \Delta g^{\mathrm{ad}}/F$ $\theta \approx 1$	$\Delta E = 0$ θ arbitrary	$\Delta E \gg \Delta g^{\mathrm{ad}}/F$ $\theta \ll 1$
$\Delta g^{\mathrm{ad}} \gg 0$ (Au)	$\varsigma^{\mathrm{ex}} - \varsigma^{\mathrm{ad}}$	ς^{ex}	ς^{ex}
$\Delta g^{\mathrm{ad}} \approx 0$ (Pt)	$\varsigma^{\mathrm{ex}} - \varsigma^{\mathrm{ad}}/2$	ς^{ex}	$\varsigma^{\mathrm{ex}} + \varsigma^{\mathrm{ad}}/2$
$\Delta g^{\mathrm{ad}} \ll 0$ (Ni)	ς^{ex}	ς^{ex}	$\varsigma^{\mathrm{ex}} + \varsigma^{\mathrm{ad}}$

The evaluation of the reaction-strain coupling coefficients ι and λ starts out with substituting Eq (13) for j^{ex} and the appropriate form of Eq (10) for θ and θ_{eq} in Eq (12) for the Faraday current, including the strain-dependent enthalpy terms. The resulting expression is then evaluated by taking the derivative with respect to e as embodied in the definitions of ι or λ, Eqs (7,8). Attention is here restricted on the representation in terms of λ, which emerges as the concise expression

$$\lambda = \left(\frac{1}{1 + \exp \frac{\Delta g^{\mathrm{ad}}}{RT}} - \frac{1}{1 + \exp \frac{\Delta g^{\mathrm{ad}} + F\Delta E}{RT}} \right) \varsigma^{\mathrm{ad}} + \varsigma^{\mathrm{ex}} . \quad (16)$$

In the limits of large negative or large positive overpotential, the limiting values of the current-strain coupling coefficient in this expression are simple combinations of electrocapillary coupling parameters.

Figures 2c) and d) illustrate the predicted mechanical modulation of the reactivity by means of qualitative graphs of $\iota(E)$ and $\lambda(E)$, respectively. With attention to λ, the most important features are nearly constant values on either side of the potential of electrosorption or underpotential deposition, E^{ad}. At E^{ad} there is a jump in λ by the amount ς^{ad}. As can be seen in the compilation of limiting values, Table I, the values of λ on each side of E^{ad} depend on the strength of adsorption of H. For the example of Au (weak adsorption), λ near equilibrium and at small magnitude of the overpotential is governed by the strain-dependence of the activation enthalpy, in other words, $\lambda \approx \varsigma^{\mathrm{ex}}$. By contrast, $\lambda \approx \varsigma^{\mathrm{ex}} - \varsigma^{\mathrm{ad}}$ for Au at large and negative overpotential.

It is remarkable that the coupling parameter λ remains well-behaved near the equilibrium potential of the reaction. Even when the current inverts its sign along with the overpotential, λ retains the constant value ς^{ex}. In other words, λ near equilibrium measures the strain-dependence of the exchange current density. By contrast, λ jumps by $-\varsigma^{\mathrm{ad}}$ when the surface undergoes the transition from dilute to concentrated adsorbate during the hydrogen electrosorption at $\Delta E = -\Delta g^{\mathrm{ad}}/F$. If we assume that the two coupling coefficients ς^{ad} and ς^{ex} are of same sign and of not too dissimilar magnitude, then the net strain-dependence of the reactivity is predicted strongest for electrodes with a negative adsorption enthalpy (as for Ni in the example of Table I) and at positive overpotential and weakest for positive adsorption enthalpy (as for Au) and at negative overpotential.

In the following Section, we discuss an experimental approach which explores the mechanical modulation of electrocatalytic reactivity and we compare first results to the theory.

III. EXPERIMENTAL PROCEDURES

The procedures of this study were largely identical to those of our earlier report on dynamic electro-chemomechanical analysis (DECMA) on polarizable electrodes, Ref. [17]. The central differences are the extension of the potential range to include the regime of hydrogen evolution and the investigation of the Faraday current modulation. In the interest of a self-contained description, we present a brief display of the procedures.

The working electrodes (WE) were 50 nm thin gold or platinum films, sputtered unto 125 μm thick polyimide (Upilex, UBE) substrates, $\approx 1 \times 2$ cm in size, with 1-2 nm titanium as an adhesion promoter. Deposition was preceded by argon plasma etching. X-ray rocking curves of films prepared in this manner reveal a strong (111)-texture [23].

The sample is mounted between clamps that serve to apply a cyclic strain. The metal WE is facing down and is contacted from below by a standing meniscus. The electrochemical cell is made from glass and has separate compartments for WE and counter electrode (CE). The reference electrode (RE), Ag/AgCl in 3.5 M KCl (World Precision Instruments), is separated from the main body of the cell by a Luggin capillary ending about 2 mm from the sample surface. The entire setup is housed in an environmental cell, which is repeatedly evacuated and purged with high purity (99.9999%) Ar and then sealed under Ar at atmospheric pressure before experiments. All potentials in this work are quoted versus the standard hydrogen electrode (SHE), and are positive by 197 mV compared to potentials measured versus Ag/AgCl [24].

As the electrolyte, all experiments used 0.5M H_2SO_4 prepared from H_2SO_4 (Suprapur, Merck) and ultrapure water (18.1 MΩ cm, Sartorius) and deaerated with 99.9999% Ar. All glassware was cleaned in 5 volume parts of concentrated H_2SO_4 + 1 part of 30% H_2O_2 for 24 hours and then rinsed thoroughly with ultrapure water. The electrode potential was controlled by a potentiostat (PG-Stat 302N AUTOLAB) equipped with a grounded working electrode, a staircase scan generator

and an impedance module.

A piezo actuator (PI-840 Physical Instruments), incorporating a displacement sensor and operated in closed-loop control mode, acts on one clamp to impose a cyclic elastic strain on the WE. The inertia of the grip system, along with heating-up of the piezoactor during fast strain cycles, limits the accessible strain frequency range to < 100 Hz.

Using the strain as the reference, the in-phase (real) and out-of-phase (imaginary) components of the amplitude of potential or current modulation was detected by means of a lock-in amplifier (SR 7270, Signal Recovery). The potential-strain response, ς, was measured in potentiostatic mode during cyclic voltammetry. As explained in Ref. [17], the lock-in amplifier here probes the potential difference between WE and RE. A delay resistance, R_D, between the WE and the potentiostate acts as a low pass filter, ensuring that the strain cycles are approximately at constant charge. Suitable values of $R_{\rm D}$ were in the range of 1 to 50 kΩ. During measurements of the current-strain response, the delay resistance was removed and the lock-in amplifier wired to measure the current modulation from the potential drop over a shunt resistance in series with the CE [17].

The primary experimental data sets are as follows: The grip displacement at any given time is read from the sensor in the piezoactor and is used as the reference signal in the lock-in amplifier. The displacement amplitude is converted into a strain amplitude, $\hat{e}$, accounting for the sample geometry and the substrate Poisson ratio [17]. The real and imaginary components of the modulation in current or potential, $\hat{I}$ or $\hat{E}$, are output data from the lock-in amplifier. With reference to Eqs (4) and (9) the coupling coefficients were computed from the data as follows:

$$\varsigma = \hat{E}_{\rm real}/\hat{e} \qquad (\text{constant } q)\,, \qquad (17)$$

$$\iota = \hat{j}_{\rm real}/\hat{e} = A^{-1}\hat{I}_{\rm real}/\hat{e} \qquad (\text{constant } E)\,, \qquad (18)$$

$$\lambda = \frac{RT}{F}\frac{\hat{I}_{\rm real}}{I\,\hat{e}} \qquad (\text{constant } E)\,, \qquad (19)$$

where I denotes the net current as measured by the potentiostate and A is the area wetted by the meniscus.

Electrochemical impedance spectroscopy (EIS) used a voltage perturbation of 10 mV. The uncompensated solution resistance, $R_{\rm U}$, was measured immediately after cyclic strain experiments using EIS in the frequency range 0.01 Hz - 1 kHz and identifying the real part of the impedance in its high-frequency limit with $R_{\rm U}$. A typical value was $R_{\rm U}$ = 18Ω. All electrode potentials shown in this work are corrected for the potential drop in solution by subtracting $I(E)R_{\rm U}$ (where I denotes the electrode current) from the nominal electrode potential value.

HER measurements typically used negative-going scans in order to minimize the accumulation of H_2 in solution. Decohesion of the metal films at large and negative potentials limited the lower vertex potentials. These were chosen so as to allow several consecutive experiments with any one sample. Tafel plots were recorded at scan rate 2mVs^{-1}, using the cyclic voltammetry staircase option with 3 mV potential step to eliminate the capacitive contribution.

IV. RESULTS

A. Samples and characterization

The HER in argon-purged 0.5M H_2SO_4 solution was studied on 111-textured thin films of gold and platinum, providing examples for weak (Au) and intermediate (Pt) hydrogen adsorption strength. The small $j^{\rm ex}$ on Au implies in particular that mass-transport limitations are benign when working in acidic solution [25].

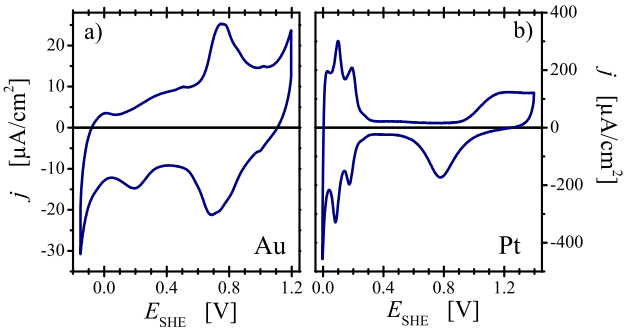

FIG. 3. Cyclic voltammogramms of current density, j, versus electrode potential, E, for **a)** Au and **b)**Pt thin film electrodes with a (111) texture in 0.5M H_2SO_4. Scan rate is 100 mV s^{-1}.

Figure 3 shows cyclic voltammograms of the Au and Pt electrodes. The data is consistent with the clean surfaces of the polycrystalline metals. Figure 4 displays the results for the HER. We shall first discuss the data for Au.

B. Gold electrode

Figure 4a) shows a Tafel plot for the gold electrode. Under forward bias (ΔE < 0), two well-defined Tafel slopes are apparent, -79 mV dec^{-1} at low overpotential magnitude ($|\Delta E|$) and -224 mV dec^{-1} at higher $|\Delta E|$. From the intersection of straight lines of best fit, the transition is found at ΔE = −0.31 V. By extrapolating the data at low $|\Delta E|$ to the equilibrium potential, the exchange current density is estimated at $j^{ex} \approx 0.08\mu$Acm^{-2}. In view of Section II the break in the Tafel graph is consistent with the signature of H electrosorption in the Heyrowsky kinetics, suggesting that for H on Au $\Delta E^{\rm ad} \approx -0.31$V.

As outlined in Section II, analysis of the DECMA data requires the separation of capacitive and Faraday effects. In this context we found it useful to inspect electrochemical impedance data. Figure 4c) shows the impedance,

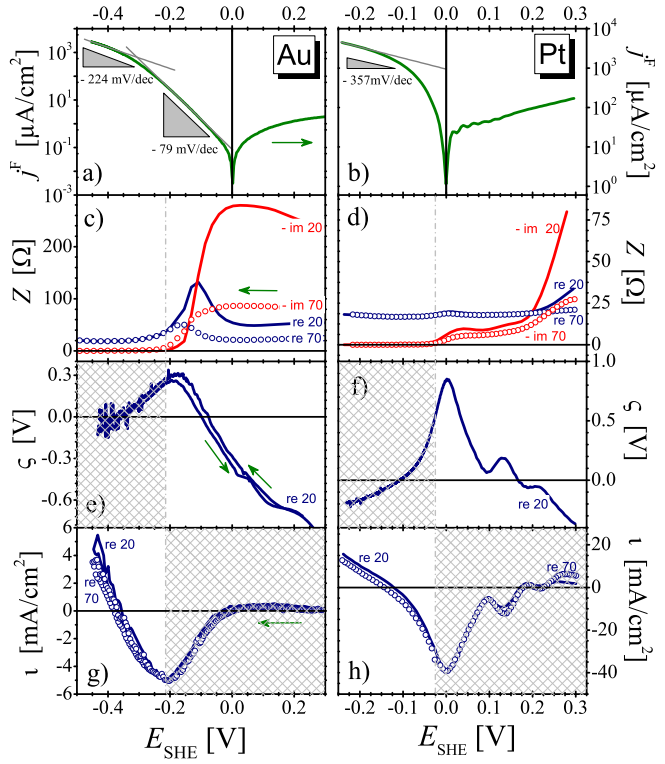

FIG. 4. Electro-chemo-mechanical characterization of Au (left column) and Pt (right column) electrodes. **a,b)**, Tafel plots of current density, j^F, versus electrode potential, E, during scans at 2 mV s^{-1}. Dashed lines are straight-line fits in regions of linear response in the log-linear representation. **c,d)** Real and imaginary parts of the impedance, Z, versus E at frequencies of 20 and 70 Hz, as indicated by labels. Vertical dash-dotted line marks transition between dominantly capacitive and dominantly Faraday currents. **e,f)** Electrocapillary coupling parameter ς at strain frequency 20 Hz and at 20 mV s^{-1} scan rate. **g,h)** Current-strain response parameter $\iota = \mathrm{d}j/\mathrm{d}e$ recorded at 20 Hz (lines) and 70 Hz (cricles) with 20 mV s^{-1} scan rate. Labels denote frequencies and distinguish real and imaginary part of response. Shaded regions mark potential regime were the respective technique is inappropriate since the requirements of dominantly capacitive (for ς) or dominantly Faraday (for ι) processes are violated.

Z, measured at the frequencies, 20 and 70 Hz, of the DECMA experiment. The key observation is a transition at $E \approx -0.2$V (dash-dotted vertical line in the left column of Fig. 4): When E is reduced below that value, the imaginary part of Z vanishes and the data loses its frequency dependence. Both aspects are signatures of the transition from a regime of dominantly capacitive processes for $E \gtrsim -0.2$V to dominantly Faraday behavior for $E \lesssim -0.2$V. This implies that DECMA data recorded for E below -0.2V is dominated by the response of the HER rate to strain, whereas the DECMA data at the more positive E is dominated by capacitive processes. Shaded regions in the graphs of Fig. 4 mark the potential regimes were the respective technique is inappropriate since the requirements of dominantly capacitive (for ς) or dominantly Faraday (for ι) processes are violated.

Results for the potential-strain response near equilibrium, as represented by the electrocapillary coupling parameter ς, are plotted in Fig. 4e). The finding of a negative value of ς at the more positive potentials agrees with results of our previous study of ς on Au in the vicinity of its pzc [17]. As the hydrogen electrosorption potential is approached, ς changes to positive. The value of ς reaches a maximum value of +0.3 V, right before the entry into the regime of dominantly Faraday behavior where the discharge of the interface by the reaction current prevents further measurement of ς by the present approach.

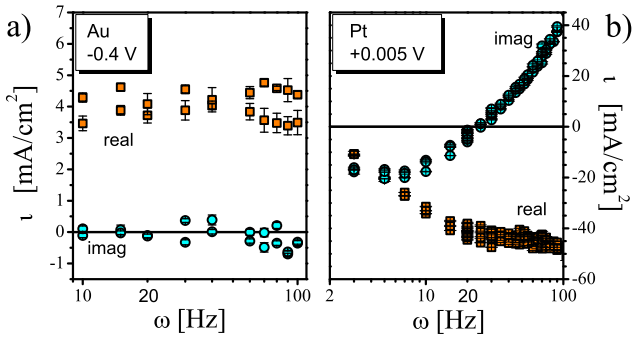

FIG. 5. Real and imaginary parts of the current-strain response parameter ι of Au and Pt electrodes versus the strain frequency ω. Potential values are indicated in legends. Data for Au is in the Faraday regime, with vanishing imaginary part. For Pt, data in the capacitive regime reveals mixed (real/imaginary) behavior at elevated frequency, consistent with results of electrochemical impedance spectroscopy.

We now turn to the strain dependence of the Faraday current. Figure 4g) displays the results for the current-strain coupling coefficient ι for frequencies 20 and 70 Hz. The frequency dependence of the current-strain response of Au has been recorded at E = -0.40 V in more detail, see Fig.5a). In agreement with Eq (5), the real part of the signal–which measures ι–is independent of the strain frequency. This supports our identification of that signal with the response of Faraday current to the cyclic strain. In particular, the real part of the current-strain response in Fig. 4g) can be identified with the Faraday current modulation when $E \lesssim -0.2V$. The data shows the parameter ι as positive-valued at the lowest end of the potential range under study. It is seen that ι decreases with increasing potential, changing sign at $E \sim -0.4V$ and then leveling off. The decrease in magnitude of the current-strain response at even more positive E may reflect capacitive behavior and so cannot be discussed as a signature of ι.

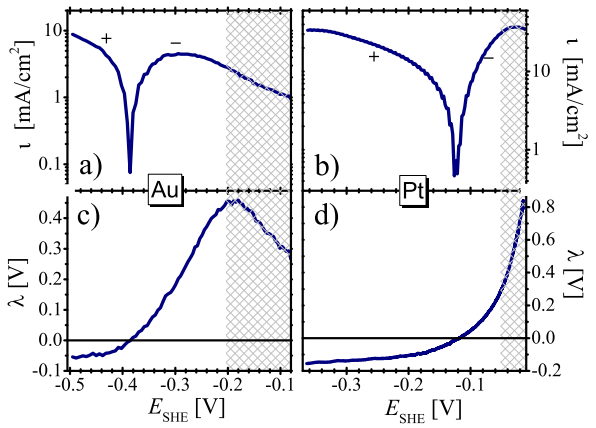

FIG. 6. Current-strain response parameters $\iota = \mathrm{d}j/\mathrm{d}e$ and $\lambda = (RT/F)\mathrm{d}\ln j^{\mathrm{F}}/\mathrm{d}e$ of Au (left) and Pt (right) as measured during negative-going potential scans at 2 mV/s. Shaded regions mark potential regime were capacitive processes dominate, preventing valid measurements of ι and λ.

Figures 6 a) and c) show results of an experiment in the HER regime, focusing on the two current-strain response parameters, ι and λ and using a slower potential scan rate (2mV/s as compared to 20 mV/s in Fig. 4) and a slightly extended potential range for closer inspection of the current-strain coupling. As above, the shaded regions in Fig. 6 mark potentials in which capacitive processes mask the Faraday-current strain response. The key observation is that the response parameters change sign near $E = -0.38$V, slightly negative of E^{ad}. In other words, at lesser overpotential magnitude the tensile strain acts to enhance the reaction current (more negative current), whereas at higher overpotential magnitude (more negative E) tensile strain acts to slow down the reaction. It is also remarkable that the parameter λ levels off in the most negative potential range, approximating a constant value $\lambda \sim -0.05$V. At higher potential λ increases, reaching the maximum value $\lambda \sim +0.45$V at the entry into the capacitive regime.

C. Platinum electrode

The Tafel plot of the Pt electrode, Fig. 4b), is curved in the entire potential range under investigation. In view of the much higher reactivity of the Pt surface, this may be attributed to transport limitations. A straight-line fit to the Tafel graph in its limit near the lower potential vertex gives a slope of $\sim -360\mathrm{mVdec}^{-1}$ and an ordinate intercept at $E = 0$ of $j \sim 0.93\mathrm{mAcm}^{-2}$.

The EIS data of Fig. 4d) show the imaginary part vanishing for $E \lesssim -0.03$V, indicating that Faraday behavior dominates in that regime, whereas pseudocapacitive processes are dominant at the higher potentials. This notion is confirmed by the potential-strain response data of Fig. 4f): The Faraday current must vanish at equilibrium, irrespective of the strain, implying $\iota = 0$ at $\Delta E = 0$. Yet, the experimental current modulation does not vanish there. In fact, the graph of the current-strain modulation exhibits an extremum at a potential only slightly positive. This agrees with a capacitive rather than Faraday process dominating the response at and above $E = 0$.

The first and second UPD peaks, at $E = 0.174$V and 0.083V in the CVs of Fig. 3 b), coincide with minima in the potential-strain response, Fig. 4f). The observed shifts of phase and sign are in agreement with those of Eqs (4) and (5), confirming that the experiment here measures the values of ς of the corresponding electrosorption processes. Similar features are not apparent in the data for Au, in agreement with the notion that Faraday processes dominate the response at the potential of H electrosorption on that metal.

The graph of current-strain response for Pt in Fig. 4h) is remarkably similar to that for Au (Fig. 4g) above), with an extremum at potentials positive of the H electrosorption potential and a sign inversion at potentials negative thereof, here at ~ -0.13V. Most notably, the sign inversion is common to both metals. For Pt, as for Au, tensile strain accelerates the reaction ($\iota < 0$) at lesser overpotentials, whereas the trend is reversed at the higher overpotentials, where tensile strain inhibits the reaction ($\iota > 0$).

Based on the electrochemical impedance data of Fig. 4d), we have identified the signals at potentials positive of -0.03V as the signatures of capacitive processes. Yet, the lack of a noticeable frequency dependence in the current-strain response data of Fig. 4h) seems to disagree with this notion. We have therefore inspected the frequency dependence of the current-strain response of Pt on in more detail, see Fig. 5 b). It can be seen that the real part of the current-strain response is only frequency-independent in the regime of $\omega \gtrsim 20$Hz. At lesser frequencies, the real part does depend on ω. Furthermore, the imaginary part is strongly frequency dependent throughout the entire frequency range under investigation. This behavior is indeed compatible with capacitive processes and not with Faraday behavior.

As for Au, we have studied the current-strain response for Pt in more detail at slower scan rate. The results, Fig. 6 b) and d), confirm the above observations. At the most negative E, the results for λ in Fig. 6 d) show only slow variation with potential, with a smallest value of $\lambda = -0.175$V.

V. DISCUSSION

The Au and Pt electrodes of our experiment probe the HER on substrates with quite different adsorption strength. Pt undergoes UPD at slightly positive overpotentials ($\Delta h^{\mathrm{ad}} \lesssim 0$), which puts it near to (but slightly to the left of) the peak of the volcano curve, Fig. 7, of exchange current density versus hydrogen enthalpy of

adsorption. By contrast, gold is way out at very positive Δh^{ad} [3, 25].

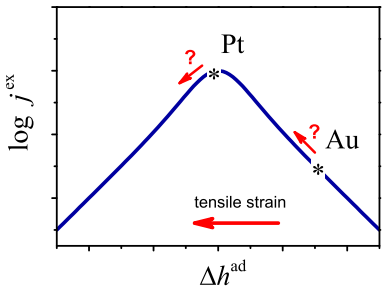

FIG. 7. Schematic representation of the position of Pt and Au on the volcano curve of exchange current density j^{ex} versus H enthalpy of adsorption, Δh^{ad} for the hydrogen evolution reaction. Tensile strain makes surface more binding for H (large arrow), which might suggest that the reactivity of Au increases while that of Pt decreases (small arrows).

Our experiments with Pt are affected by the transport limitations which ensue from the large Faraday current densities and which impair the discussion of the experimental kinetics in terms of simple models, such as the Heyrowsky model of our theory section. The impact of solution resistance can be mitigated by focusing on the coupling parameter λ, which is defined as the *relative* change of the current in response to strain. Since the resistance acts on j^{F} as well as δj^{F}, its impact is partly canceled when evaluating $\delta j^{\mathrm{F}}/j^{\mathrm{F}}$. In this sense, λ is an inherently robust parameter even when the current is affected by the solution resistance. Yet, Pt presents the additional challenge that the strong capacitive signals of hydrogen UPD nearly coincide with the equilibrium of the HER, complicating the separation of the modulated Faraday current. As a consequence of the more challenging nature of the experiments with Pt, the discussion of this first study focuses on the findings for Au.

A. Electrosorption potential and Tafel slope

Our experiments for gold indicate Tafel slopes of -79 mV dec^{-1} at low overpotential magnitude ($|\Delta E|$) and -224 mV dec^{-1} at higher $|\Delta E|$, with a break at around E = −0.31V and an exchange current density $j^{ex} \approx 0.08 \mu\mathrm{Acm}^{-2}$. These values will now be discussed in relation to the literature.

For the idealized case of symmetry factor 1/2, the Tafel slopes of the Heyrowsky reaction of Eq (12) correspond to $\mathrm{d}\ln j^{\mathrm{ex}}/\mathrm{d}E = -3F/(2RT)$ or -40 mV/dec and $-F/(2RT)$ or -119 mV/dec at low and high overpotential magnitudes, respectively. The factor three difference between the slopes in the respective regimes agrees with our experimental observations. Yet, the absolute values of the experiment are consistently higher than the prediction. It is therefore remarkable that previous experimental studies of the HER on polycrystalline gold found Tafel slopes that do agree with the Heyrowsky model, namely -49 ± 19 mV dec^{-1} and -122 ± 11 mV dec^{-1} at low and high overpotential, respectively [26–30].

The change in Tafel slope is an inherent feature of the Heyrowsky kinetics, where it demarcates the transition between dilute and concentrated hydrogen coverage at the electrosorption potential, $\Delta E^{\mathrm{ad}} = -\Delta g^{\mathrm{ad}}/F$. Our observation of the Tafel break at ~ E = −0.31V suggests that the free energy of hydrogen adsorption on Au is Δg^{ad} = +0.31 eV or +29kJmol^{-1}. Ab initio computations for H on Au(111) put Δg^{ad} at +0.45eV [3] and 0.41eV [31]. Furthermore, Δg^{ad} reflects the metal-hydrogen bond strength, which for Au has been reported 0.50eV more positive than for Pt [32]. This latter value would suggest that $E^{\mathrm{ad}} \approx$ -0.3 to -0.4 V in view of the H UPD signatures on Pt at +0.1 to +0.2V, see Fig. 3. It is seen that the observed potential of -0.31 eV puts the Tafel break in our data within the interval of reported values for the electrosorption potential of H. Furthermore, the exchange current density for the Au electrode in our experiment, $j^{\mathrm{ex}} \approx 0.08 \mu\mathrm{Acm}^{-2}$, agrees well with the values 0.08 $\mu\mathrm{Acm}^{-2}$ in Ref. [20] and 0.12 $\mu\mathrm{Acm}^{-2}$ in Ref. [25].

To summarize these observations, our results overestimate the Tafel slopes, but provide values for the apparent adsorption potential ΔE^{ad} and for the exchange current density j^{ex} that are consistent with previous reports. We attribute the deviation in Tafel slope to transport limitations, but conclude from the agreement of ΔE^{ad} and j^{ex} that the impact of the solution resistance is limited and that our data for Au give a reasonable qualitative representation of the inherent kinetics of the reaction.

Because of the more severe transport limitations, we refrain from discussing the Pt data in detail. However, we recall that the qualitative behavior of $\iota(E)$ of Pt is found similar to Au. This lends qualitative support to our discussion of the impact of strain on the reactivity at Au surface.

B. Potential-strain response

As argued in Section IV C, our data for potential- and current modulation with strain for both electrodes are consistent with a transition between dominantly capacitive or pseudocapacitive behavior at the more positive potentials and dominantly Faraday behavior at more negative potential. The respective regimes allow, exclusively, the measurement of the potential-strain response at constant charge (pseudocapacitive processes) and of the current-strain response at constant potential (Faraday processes).

Previous work has found that $\varsigma < 0$ for capacitive processes with little chemisorption on transition and noble metal surfaces and specifically on Au [12–17]. This is born out by the present results at the most positive potentials. During negative-going scans, as the potential approaches E^{ad} from above, pseudocapactive adsorption

of H will become more important and eventually dominate the potential-charge and potential-strain response. In view of the definition of $\varsigma^{\rm ad}$, Eq (14), the experimental potential-strain response parameter will then gradually change; when chemisorption dominates the response will eventually take on the value of $\varsigma^{\rm ad}$ [7]. In view of the change of sign in ς and its continuing increase upon decreasing the potential (Fig. 4 e), we therefore conclude that $\varsigma^{\rm ad}$ of H on Au is positive valued with a lower bound of +0.3V. The finding for Au is consistent with positive values of ς during H underpotential deposition (UPD) on Pd [7, 33] and Pt [7, 13]. The positive $\varsigma^{\rm ad}$ imply that tensile strain makes the metal surfaces more binding for hydrogen.

C. Current-strain response

For the current-strain response our results indicate that the graphs of $\lambda(E)$ for both, Pt and Au, agree well with the model of Section II, specifically inasmuch as *i.*) both surfaces display the change of sign in $\lambda(E)$, *ii.*), $\lambda(E)$ becomes approximately constant in the limit of large negative overpotential, and *iii.*) the change in sign is at a potential negative of $E^{\rm ad}$. We take these observation as a confirmation of the concept of a strain-dependent Heyrowsky reaction, as explored by our theory. Details will now be addressed.

The central finding for the current-strain response on Au is that λ changes sign at $E \approx -0.38$V, around 70 mV negative of $E^{\rm ad}$. At lesser $|\Delta E|$, the negative value of λ implies that tensile strain enhances the reactivity, whereas $\lambda > 0$ at higher $|\Delta E|$ means that tensile strain here diminishes the reactivity. The same qualitative behavior is found for Pt, except that the change in sign of λ here occurs much closer to the equilibrium potential of the HER.

Upon comparing Figs. 1 and 6 it is seen that the graphs of ι and λ in theory and experiment agree well if, for Au, we take $\varsigma^{\rm ex}$ of same sign as and moderately lesser magnitude than $\varsigma^{\rm ad}$. In view of Table I, the constant value of $\lambda \approx -0.05$V at negative overpotential implies that $\varsigma^{\rm ex} - \varsigma^{\rm ad} \approx -0.05$V. The current-strain coupling reaches a maximum value of $\lambda = +0.4$V at the transition between capacitive and Faraday behavior, implying $\varsigma^{\rm ex} \geq +0.4$V and, therefore, $\varsigma^{\rm ad} \geq +0.45$V. This is also consistent with the finding for the potential-strain coupling, which tends to increase with decreasing potential, reaching a maximum value $\varsigma = +0.3V$ before the transition to Faraday behavior prevents further observation with the present technique.

The observation of $|\varsigma^{\rm ad}| \gtrsim |\varsigma^{\rm ex}|$ appears indeed natural if we take the enthalpies of adsorbed H and of the transition state to be coupled via a Brønsted-Evans-Polanyi relation [4, 34–36]. DFT data for adsorption on different substrates reveal a scaling factor, connecting $\Delta h^{\rm ex}$ to $\Delta h^{\rm ad}$, near to but slightly less than unity [36]. This is consistent with present observation for surfaces under different states of strain.

Inasmuch as the results for Pt provide a qualitative description of the current-strain coupling, we conclude that the reactivity at finite overpotential here also decreases with tensile strain. The apparent change in sign of λ, quite close to the transition to capacitive behavior, may suggest that the exchange current density as defined through Eq (12) shows the opposite trend, with enhanced current under strain in tension. However, empirical values for $j^{\rm ex}$ are typically derived by extrapolation from currents at finite overpotential to $\Delta E = 0$. The $j^{\rm ex}$ measured in this way depends on strain through the current in the regime where $\lambda < 0$. We therefore conclude that the strain dependence of the 'empirical' HER exchange current on Pt is governed by λ at finite overpotential, which implies here that the reaction kinetics is inhibited by tensile strain.

According to the results of Table I, $\lambda < 0$ for Pt under finite forward bias requires that $\varsigma^{\rm ex} < \varsigma^{\rm ad}/2$. This would imply that the difference between the two electrocapillary coupling parameters ς is here larger than on Au surfaces.

At first sight, the observations that tensile strain inhibits the reactivity of both, Au and Pt under forward bias are not immediately obvious if one considers the volcano curve (Fig. 7) for the reactivity - as represented by the exchange current density - of metal surface for the HER. Since tensile strain makes the surface more binding for H, it shifts both Au and Pt to lesser $\Delta h^{\rm ad}$ on the graph. With Au on the descending branch of the volcano and Pt near to its top, a finite tensile strain would make Au more reactive and Pt less reactive, contrary to the observation. The apparent discrepancy is related to the different strain dependence of two measures for the reactivity, namely the exchange current density on the one hand and the Faraday current at finite overpotential on the other. Our discussion of the results for Au indicates that the exchange current density is indeed enhanced by tensile strain since $\lambda \approx \varsigma^{\rm ex}$, which is positive. Yet, significant current can only be obtained at higher overpotential, where the hydrogen coverage has changed from dilute to concentrated. Here, the theory indicates $\lambda \approx \varsigma^{\rm ex} - \varsigma^{\rm ad}$, which takes on negative values.

VI. CONCLUSION

In this study we have inspected the consequences of elastic strain of an electrode on its electrocatalytic activity for the hydrogen evolution reaction. Starting out with the kinetic rate equation for the Heyrowski reaction, we introduced separate coupling coefficients, $\varsigma^{\rm ad}$ and $\varsigma^{\rm ex}$, respectively, for the strain dependence of the adsorption enthalpy of H and for the activation energy. The relative change of the Faraday current in response to strain can be quantified by the parameter λ, which emerges as a weighted sum of the two coupling coefficients. The weighting factors depend on the overpotential, ΔE. Near equilibrium ($\Delta E = 0$) we find $\lambda = \varsigma^{\rm ex}$, so that the current

modulation is entirely governed by the strain dependence of the transition state energy. By contrast, the reactivity at higher overpotentials can also reflect the strain-dependence of the adsorption enthalpy as measured by ς^{ad}. The coupling far from equilibrium depends on the sign of ΔE and on the strength of H adsorption. As a consequence of the Brønsted-Evans-Polanyi relation, it appears natural to expect ς^{ad} and ς^{ex} to be of same sign, with a larger magnitude for ς^{ad}.

Our experiment explores an approach towards monitoring the mechanical modulation of electrocatalytic reactions in experiment by using a small cyclic strain of the electrode and a lock-in technique to detect the ensuing modulation of the reaction current. It can be applied simultaneously with the potential scan which is used to obtain data for a Tafel plot. While the absence of forced liquid flow – as in a rotating disk experiment – impairs the results in the present implementation, meaningful data was obtained for the exchange current density and the electrosorption potential of the HER on Au.

The variation of λ with ΔE exhibits qualitatively similar behavior for Au and Pt, with $\lambda < 0$ at large and negative overpotential (i.e., forward bias of the HER) and a transition to $\lambda > 0$ near the H electrosorption potential. The transition is consistent with our theory. For Au as well as Pt, we find tensile strain to reduce the reactivity under sufficiently large forward bias. By contrast, the two metals may differ in respect to the impact of strain on the exchange current density: while j^{ex} of Au increases under tensile strain, the data are at least compatible with j^{ex} of Pt decreasing. The strain-dependence of j^{ex} is in agreement with expectation based on the position of the two elements on the volcano curve of j^{ex} versus H adsorption enthalpy. Yet, the different behavior of the reactivity under finite bias shows that the strain effect on the reaction kinetics is governed by additional factors, which are not appropriately measured by the exchange current alone.

In principle, our approach towards monitoring mechanically modulated reaction rates in electrocatalysis can be applied quite generally to electrocatalytic reactions. It may thus evolve into a new tool for studying strain-dependent catalysis and for linking the relevant phenomena to models of the underlying microscopic processes.

Qibo Deng acknowledges support by the Chinese Scholarship Council.

[1] A. Ruban, B. Hammer, P. Stoltze, H. L. Skriver and J. K. Nørskov, J. Mol. Catal. A: Chem. 1997, 115, 421.
[2] M. Mavrikakis, B. Hammer and J. K. Nørskov, Phys. Rev. Lett. 1998, 28, 2819.
[3] J. K. Nørskov, T. Bligaard, A. Logadottir, J. R. Kitchin, J. G. Chen, S. Pandelov, U. Stimming, J. Electrochem. Soc. 2005, 152, J23.
[4] T. Bligaard, J. K. Nørskov, S. Dahl, J. Matthiesen, C. H. Christensen and J. Sehested, J. Catal. 2004, 224, 206.
[5] A. Schlapka, M. Lischka, A. Groß, U. Käsberger, P. Jakob, Phys. Rev. Lett. 2004, 91, 016101.
[6] L. A. Kibler, A. M. El-Aziz, R. Hoyer, and D. M. Kolb, Angew. Chem. Internat. Ed. 2005, 44, 2080.
[7] J. Weissmüller, R. N. Viswanath, L. A. Kibler, D. M. Kolb, Phys. Chem. Chem. Phys. 2011, 13, 2114.
[8] Shao, M.; Liu, P.; Zhang, J.; Adzic, R. J. Phys. Chem. B 2007, 111, 6772.
[9] L. A. Kibler, Electrochimica Acta 2008, 53, 6824.
[10] Strasser, P.; Koh, S.; Anniyev, T.; Greeley, J.; More, K.; Yu, C. F.; Liu, Z. C.; Kaya, S.; Nordlund, D.; Ogasawara, H.; Toney, M. F.; Nilsson, A. Nature Chemistry 2010, 2, 454.
[11] A.Ya. Gokhshtein, Russ. Chem. Rev., 1975, 44, 921.
[12] W. Haiss, Rep. Prog. Phys. 2001, 64, 591.
[13] R.N. Viswanath, D. Kramer, J. Weissmüller, Electrochim. Acta. 2008, 53, 2757.
[14] M. Smetanin, R.N. Viswanath, D. Kramer, D. Beckmann, T. Koch, L.A. Kibler, D.M. Kolb, J. Weissmüller, Langmuir 2008, 24, 8561.
[15] F. Weigend, F. Evers, J. Weissmüller, Small 2006, 2, 1497.
[16] Y. Umeno, C. Elsässer, B. Meyer, P. Gumbsch, M. Nothacker, J. Weissmüller, F. Evers, EPL, 2007, 78, 13001.
[17] M. Smetanin, Q. Deng and J. Weissmüller, Phys. Chem. Chem. Phys. 2011, 13, 17313.
[18] J. Weissmüller, D. Kramer, Langmuir 2005, 21, 4592.
[19] S. Trasatti, J. Electroanal. chem. 1972, 39, 163.
[20] G. J. Brug, M. Sluyters-Rehbach, J. H. Sluters, A. Hamelin, J. Electroanal. Chem. 1984, 181, 245.
[21] R. Parsons, Trans. Faraday Soc., 1958, 54, 1053.
[22] W. Sheng, H. A. Gasteiger and Y. Shao-Horn, J. Electrochem. Soc. 2010, 157, 1529.
[23] M. Smetanin, Mechanics of electrified interfaces in diluted electrolytes, dissertation, Universität des Saarlandes, 2010. urn:nbn:de:bsz:291-scidok-33803.
[24] A.J. Bard, L.R. Faulkner, Electrochemical Methods, 2nd edition (Wiley, New York 2001).
[25] L.A. Kibler, Chem. Phys. Chem. 2006, 7, 985.
[26] M.N. Dešić, M.M. Popovic, M.D. Obradovic, Lj.M. Vracar and B.N. Grgur, J. Serb. Chem. Soc. 2005, 70, 231.
[27] G.M. Schmid, Electrochim. Acta. 1967, 12, 449.
[28] A. T. Khun and M. Byrne, Elcctrochim. Acta. 1971, 16, 391.
[29] J. Perez, E. R. Gonzalez, and H. M. Villullas, J. Phys. Chem. B 1998, 102, 10931.
[30] B.E. Conway and L. Bai, Electrochim. Acta. 1986, 31, 1013.
[31] E. Santos, A. Lundin, K. Ptting, P. Quaino, and W. Schmickler, Phys. Rev. B 2009, 79, 235436.
[32] J. Greeley and M. Mavrikakis, Nat. Mater. 2004, 3, 810.
[33] J. W. Shin, U. Bertocci, G. R. Stafford, J. Electrochem. Soc. 2011, 158, F127.
[34] J. N. Brønsted, Chemical Reviews 1928, 5, 231.
[35] M. G. Evans and M. Polanyi, Transactions of the Faraday Society 1938, 34, 11.
[36] J. K. Nørskov et al., J. Catalysis 2002, 209, 275.

Figure for Table of Contents